Supporting Information

Dalchau et al. 10.1073/pnas.1015452108

SI Materials and Methods

Numerical Integration of the Three-Loop Model Equations. The three-loop model (1) of the central oscillator was used to investigate the source of dynamical differences between plants grown with and without exogenous sucrose in the growth media. The model equations are a system of nonlinear differential equations,

$$\frac{dx}{dt} = f(x, p, \Theta_{\text{light}}), \qquad \text{[S1]}$$

where $x \in \mathbb{R}^{16}$ is the vector of concentrations, $p \in \mathbb{R}^{77}$ are the kinetic rate parameters, and Θ_{light} is a boolean variable representing the availability of light. Throughout this work, we considered altered parameter sets $\hat{p} \in \mathbb{R}^{77}$, where each $\hat{p}_i$ is equal to $p_i^{\text{r}} p_i$, and p_i^{r} is the relative value of parameter p_i. Note if p^{r} is the vector of 1s, then $\hat{p}$ is equal to the nominal parameter set p. The model equations were solved numerically using MATLAB's *ode15s* stiff equation solver (2). The concentrations of mRNA and protein (nuclear and cytoplasmic) were initialized as the vector of 1s. With this arbitrary choice, all of the simulations converged asymptotically to the desired limit cycle.

Period and Amplitude Plots for Associating Exogenous Sucrose Availability with Single Model Parameter Alterations. Period and amplitude (oscillation fold ratio) in constant light (LL) and constant dark (DD) were computed for $p_i^{\text{r}} = 10^a$ for all i, with $a = -2, -1.99, -1.98, \ldots, 2$. The q_is and the light protein parameters p_5, m_{15}, and k_{13} were not considered, as they do not influence the state trajectory in constant conditions. The model equations were simulated for 600 h in both LL and DD, with the *refine* option in the *odeset* defined as 10. (The *refine* option set to a value n simply generates n times as many points, independently of the solver tolerances. Refining the solution vectors enables a more accurate prediction of the time and value of peak and trough values in an oscillation, of particular importance when computing period and amplitude from a numerical solution of differential equations.) The peak and trough values of [*LHY/CCA1* mRNA] (the choice of state variable is arbitrary for computation of period, although [*LHY/CCA1* mRNA] was selected because our earliest observations that motivated this work came from measurements of *CCA1::luc* luminescence) were then located and used to evaluate period and amplitude. Period was taken as the difference in time of the final two peak values, whereas the amplitude was expressed as the fold ratio between the last peak and trough values. An example of the period and oscillation fold ratio is given for n_5 (maximum light-independent rate of *Y/GI* transcription) in Fig. S2*A*.

Single-parameter alterations that resulted in the LL period between 20 and 30 h and the DD oscillation fold ratio <1.1 were considered candidates (Fig. S2*B*). Simulated outputs from the candidate single-parameter alterations were then classified by way of a *K*-means clustering algorithm (3) (Fig. S2*C*). The model equations were simulated for two cycles (48 h) of 12 h light, 12 h dark (L12/D12) before DD for 120 h. Numerical solutions for [*LHY/CCA1* mRNA] were obtained in 0.2-h increments for analysis with the *K*-means algorithm. The *kmeans* function in the Statistics Toolbox for MATLAB (4) was used to implement the algorithm, setting the distance measure to $1 - \rho$, where ρ is the cross-correlation coefficient. The correlation distance measure enabled scale-free clustering with respect to the shape of the simulated outputs.

Simulated Annealing Algorithm for Fine-Tuning Model Parameters. The three-loop model of the central oscillator (1) was again used to investigate potential roles for sugar signaling in the plant circadian clock. *Luciferase* luminescence data from plants grown without exogenous sucrose in the growth media were used to reestimate the model parameters. Only the parameters that define the light input protein (p_5, m_{15}, k_{13}, and q_3) were excluded from this analysis, leaving 73 model parameters to assign. We designed an optimization algorithm that minimized the difference between the measured luminescence data and model simulated output.

The combinatorial complexity involved in an optimization problem over 73 parameters is vast and almost untenable. To reduce the size of the parameter space, we rescaled the state variables by dividing each one by its corresponding Michaelis degradation constant k_i, resulting in a reduction in the size of the parameter space to 63 parameters. Let $c_L^{(m)} = k_1 \hat{c}_L^{(m)}$, $c_L^{(c)} = k_2 \hat{c}_L^{(c)}$, etc. By defining ρ_i ($i = L, T, X, Y, A$) as the ratio between the cytoplasmic and nuclear protein scales (i.e., k_2/k_3 for LHY), and applying some parameter rescalings (Table S3), the model equations become

$$\frac{d\hat{c}_L^{(m)}}{dt} = \left(\frac{\hat{g}_0^{\alpha}}{\hat{g}_0^{\alpha} + \hat{c}_A^{(n)^{\alpha}}}\right)\left(\Theta_{\text{light}}(t)\left(\hat{q}_1 \hat{c}_P^{(n)} + \hat{n}_0\right) + \frac{\hat{n}_1 \hat{c}_X^{(n)^a}}{\hat{g}_1^a + \hat{c}_X^{(n)^a}}\right) - \frac{\hat{m}_1 \hat{c}_L^{(m)}}{1 + \hat{c}_L^{(m)}} \qquad \text{[S2]}$$

$$\frac{d\hat{c}_L^{(c)}}{dt} = \hat{p}_1 \hat{c}_L^{(m)} - r_1 \hat{c}_L^{(c)} + \hat{r}_2 \hat{c}_L^{(n)} - \frac{\hat{m}_2 \hat{c}_L^{(c)}}{1 + \hat{c}_L^{(c)}} \qquad \text{[S3]}$$

$$\frac{d\hat{c}_L^{(n)}}{dt} = \rho_L\left(r_1 \hat{c}_L^{(c)} - \hat{r}_2 \hat{c}_L^{(n)}\right) - \frac{\hat{m}_3 \hat{c}_L^{(n)}}{1 + \hat{c}_L^{(n)}} \qquad \text{[S4]}$$

$$\frac{d\hat{c}_T^{(m)}}{dt} = \left(\frac{\hat{n}_2 \hat{c}_Y^{(n)^b}}{\hat{g}_2^b + \hat{c}_Y^{(n)^b}}\right)\left(\frac{\hat{g}_3^c}{\hat{g}_3^c + \hat{c}_L^{(n)^c}}\right) - \frac{\hat{m}_4 \hat{c}_T^{(m)}}{1 + \hat{c}_T^{(m)}} \qquad \text{[S5]}$$

$$\frac{d\hat{c}_T^{(c)}}{dt} = \hat{p}_2 \hat{c}_T^{(m)} - r_3 \hat{c}_T^{(c)} + \hat{r}_4 \hat{c}_T^{(n)} - \left(\left(1 - \Theta_{\text{light}}(t)\right)\hat{m}_5 + \hat{m}_6\right)\frac{\hat{c}_T^{(c)}}{1 + \hat{c}_T^{(c)}} \qquad \text{[S6]}$$

$$\frac{d\hat{c}_T^{(n)}}{dt} = \rho_T\left(r_3 \hat{c}_T^{(c)} - \hat{r}_4 \hat{c}_T^{(n)}\right) - \left(\left(1 - \Theta_{\text{light}}(t)\right)\hat{m}_7 + \hat{m}_8\right)\frac{\hat{c}_T^{(n)}}{1 + \hat{c}_T^{(n)}} \qquad \text{[S7]}$$

$$\frac{d\hat{c}_X^{(m)}}{dt} = \frac{\hat{n}_3 \hat{c}_T^{(n)^d}}{\hat{g}_4^d + \hat{c}_T^{(n)^d}} - \frac{\hat{m}_9 \hat{c}_X^{(m)}}{1 + \hat{c}_X^{(m)}} \qquad \text{[S8]}$$

$$\frac{d\hat{c}_X^{(c)}}{dt} = \hat{p}_3\hat{c}_X^{(m)} - r_5\hat{c}_X^{(c)} + \hat{r}_6\hat{c}_X^{(n)} - \frac{\hat{m}_{10}\hat{c}_X^{(c)}}{1+\hat{c}_X^{(c)}} \quad \text{[S9]}$$

$$\frac{d\hat{c}_X^{(n)}}{dt} = \rho_X\left(r_5\hat{c}_X^{(c)} - \hat{r}_6\hat{c}_X^{(n)}\right) - \frac{\hat{m}_{11}\hat{c}_X^{(n)}}{1+\hat{c}_X^{(n)}} \quad \text{[S10]}$$

$$\frac{d\hat{c}_Y^{(m)}}{dt} = \left(\Theta_{\text{light}}(t)\hat{q}_2\hat{c}_P^n + \frac{\left(\Theta_{\text{light}}(t)\hat{n}_4 + \hat{n}_5\right)\hat{g}_5^e}{\hat{g}_5^e + \hat{c}_T^{(n)^e}}\right) \times \left(\frac{\hat{g}_6^f}{\hat{g}_6^f + \hat{c}_L^{(n)^f}}\right) - \frac{\hat{m}_{12}\hat{c}_Y^{(m)}}{1+\hat{c}_Y^{(m)}} \quad \text{[S11]}$$

$$\frac{d\hat{c}_Y^{(c)}}{dt} = \hat{p}_4\hat{c}_Y^{(m)} - r_7\hat{c}_Y^{(c)} + \hat{r}_8\hat{c}_Y^{(n)} - \frac{\hat{m}_{13}\hat{c}_Y^{(c)}}{1+\hat{c}_Y^{(c)}} \quad \text{[S12]}$$

$$\frac{d\hat{c}_Y^{(n)}}{dt} = \rho_Y\left(r_7\hat{c}_Y^{(c)} - \hat{r}_8\hat{c}_Y^{(n)}\right) - \frac{\hat{m}_{14}\hat{c}_Y^{(n)}}{1+\hat{c}_Y^{(n)}} \quad \text{[S13]}$$

$$\frac{dc_P^{(n)}}{dt} = (1-\Theta_{\text{light}}(t))p_5 - \frac{m_{15}\hat{c}_P^{(n)}}{k_{13}+\hat{c}_P^{(n)}} - q_3\Theta_{\text{light}}(t)\hat{c}_P^{(n)} \quad \text{[S14]}$$

$$\frac{d\hat{c}_A^{(m)}}{dt} = \Theta_{\text{light}}(t)\hat{q}_4\hat{c}_P^n + \frac{\hat{n}_6\hat{c}_L^{(n)^g}}{\hat{g}_7^g + \hat{c}_L^{(n)^g}} - \frac{\hat{m}_{16}\hat{c}_A^{(m)}}{1+\hat{c}_A^{(m)}} \quad \text{[S15]}$$

$$\frac{d\hat{c}_A^{(c)}}{dt} = \hat{p}_6\hat{c}_A^{(m)} - r_9\hat{c}_A^{(c)} + \hat{r}_{10}\hat{c}_A^{(n)} - \frac{\hat{m}_{17}\hat{c}_A^{(c)}}{1+\hat{c}_A^{(c)}} \quad \text{[S16]}$$

$$\frac{d\hat{c}_A^{(n)}}{dt} = \rho_A\left(r_9\hat{c}_A^{(c)} - \hat{r}_{10}\hat{c}_A^{(n)}\right) - \frac{\hat{m}_{18}\hat{c}_A^{(n)}}{1+\hat{c}_A^{(n)}} \quad \text{[S17]}$$

For the cost function, we took the standard LSQ (least squares) approach, minimizing the 2-norm of the residuals between data and simulated output,

$$\Delta_{\text{LSQ}}(p) := \sum_{d\in D}\sum_{i=1}^{N_d} e(p)/N_d, \quad \text{[S18]}$$

where $\mathcal{D}$ is the set of *luc* luminescence data, N_d is the number of observations in experiment $d \in \mathcal{D}$, and $e(p)$ is the residual between data and simulated model output with parameters p. The denominator N_d ensures an equal contribution from each experiment, irrespective of the number of observations. As the experimental data used could not be calibrated to actual concentrations of mRNA, we assumed that the measured luminescence is a linear function of [mRNA] (5). Therefore, we define the residual norm e by solving a linear regression problem,

$$e(p) := \min_{a,b} \| ax_d(p) + b - y_d \|_2, \quad \text{[S19]}$$

where y_d is the vector of *luciferase* luminescence measurements from dataset d, and x_d is the corresponding simulated output. This scheme ensures that the dynamics of the optimized model are not constrained by the signal strength of the *luc* reporter system.

Δ_{LSQ} (Eq. S18) was evaluated by first obtaining numerical solutions for [*LHY/CCA1* mRNA] and [*TOC1* mRNA] at the time points corresponding to the LL and DD *luc* luminescence data. The *polyfit* function in MATLAB was then used to find the minimizers a and b in Eq. S19 to compute $e(p)$ for each dataset, which were then substituted into Eq. S18 to find $\Delta_{\text{LSQ}}(p)$.

Local minima of the cost function (Eq. S18) were often found to exhibit oscillations with multiple periods in entrained L16/D8 or L8/D16 cycles, photoperiodic conditions not investigated in this cost function. Therefore, a second term was added to the cost function (Eq. S18) to penalize systems that generated trajectories with multiple periods in these alternative photoperiods. The model equations (Eqs. S2–S17) were simulated under L16/D8 and L8/D16 conditions for 840 h, and the first 600 h were discarded as transitory in each case. The times of local maxima and minima of simulated [*TOC1* mRNA] were then computed for $t \in [600\ 840]$, as $t_{\max}^{(1)}, t_{\max}^{(2)}, \ldots, t_{\max}^{(p)}$ and $t_{\min}^{(1)}, t_{\min}^{(2)}, \ldots, t_{\min}^{(q)}$, respectively. Then, allowing for biphasic oscillations, we defined the entrainment cost term as

$$\Delta_{\text{ent}}^{\text{LD}}(p) := \left\| \begin{pmatrix} t_{\max}^{(5)} \\ t_{\max}^{(6)} \\ \vdots \\ t_{\max}^{(p)} \end{pmatrix} - \begin{pmatrix} t_{\max}^{(1)} \\ t_{\max}^{(2)} \\ \vdots \\ t_{\max}^{(p-4)} \end{pmatrix} \right\|_2 + \left\| \begin{pmatrix} t_{\min}^{(5)} \\ t_{\min}^{(6)} \\ \vdots \\ t_{\min}^{(q)} \end{pmatrix} - \begin{pmatrix} t_{\min}^{(1)} \\ t_{\min}^{(2)} \\ \vdots \\ t_{\min}^{(q-4)} \end{pmatrix} \right\|_2 \quad \text{[S20]}$$

for LD as L16/D8 and L8/D16. Therefore, the complete cost function is

$$\Delta(p) = \Delta_{\text{LSQ}}(p) + \Delta_{\text{ent}}^{\text{L16/D8}}(p) + \Delta_{\text{ent}}^{\text{L8/D16}}(p). \quad \text{[S21]}$$

A Metropolis–Hastings simulated annealing algorithm (6) was used to find parameter sets p that minimized $\Delta(p)$. As is customary in simulated annealing, the cooling parameter was taken to be a linear function of the iteration number. In addition, we applied an adaptive cooling method on the search direction. At each iteration, we propose a random search direction in an N-dimensional projection p^N comprised of N randomly chosen parameters, where $N := \lceil \alpha\Delta \rceil$, and α is constant. Each p_i was moved to $\hat{p}_I$, which is Gaussian distributed with mean p_i and variance σ^2, where $\sigma := \beta\Delta$ and β is constant. This procedure was done to enable automatic fine-tuning of the parameters as we approach a local minimum of the cost function.

Mathematical Characterization of the Light/Dark-Dependent Degradation of GI. The three-loop model equations were modified to reflect the dark-dependent degradation of Y (GI) protein observed in ref. 7. The equations for cytoplasmic and nuclear Y (GI) protein become

$$\frac{dc_Y^{(c)}}{dt} = p_4c_Y^{(m)} - r_7c_Y^{(c)} + r_8c_Y^{(n)} - \left((1-\Theta_{\text{light}}(t))\hat{m}_{13} + m_{13}\right)\frac{c_Y^{(c)}}{k_{11}+c_Y^{(c)}} \quad \text{[S22]}$$

$$\frac{dc_Y^{(n)}}{dt} = r_7c_Y^{(c)} - r_8c_Y^{(n)} - \left((1-\Theta_{\text{light}}(t))\hat{m}_{14} + m_{14}\right)\frac{c_Y^{(n)}}{k_{12}+c_Y^{(n)}}, \quad \text{[S23]}$$

where $\hat{m}_{13}$ and $\hat{m}_{14}$ are the dark-dependent degradation rates of *Y* (*GI*) protein in the cytoplasm and the nucleus, respectively. The new kinetic parameters were defined in terms of the light/dark-independent counterparts m_{13} and m_{14} as

$$\widehat{m}_{13} := dm_{13}, \widehat{m}_{14} := dm_{14}, \qquad \textbf{[S24]}$$

where d is a dimensionless parameter to assign, representing the relative rate of dark-dependent GI protein degradation.

1. Locke JC, et al. (2006) Experimental validation of a predicted feedback loop in the multi-oscillator clock of Arabidopsis thaliana. *Mol Syst Biol* 2:59.
2. Shampine LF, Reichelt MW (1997) The MATLAB ODE suite. *SIAM J Sci Comput* 18:1–22.
3. MacQueen J (1967) Some methods for classification and analysis of multivariate observations. *Proc Fifth Berkeley Symp Math Stat Prob* 1:281–297.
4. Seber GAF (2004) *Multivariate Observations* (Wiley, New York).
5. Finkenstädt B, et al. (2008) Reconstruction of transcriptional dynamics from gene reporter data using differential equations. *Bioinformatics* 24:2901–2907.
6. Brooks SP, Morgan BJT (1995) Optimization using simulated annealing. *Statistician* 44: 241–257.
7. David KM, Armbruster U, Tama N, Putterill J (2006) Arabidopsis GIGANTEA protein is post-transcriptionally regulated by light and dark. *FEBS Lett* 580:1193–1197.

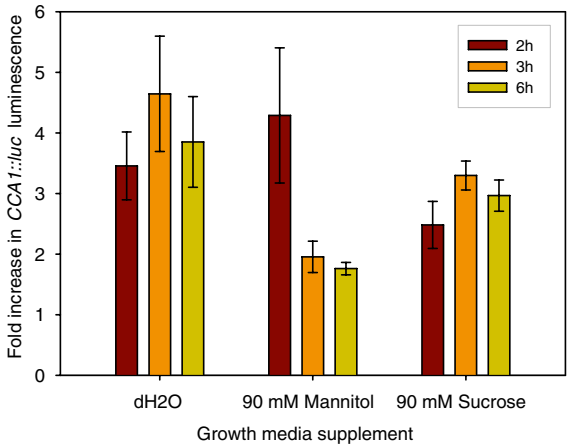

Fig. S1. Cold induces *CCA1* promoter activity after 60 h of darkness. *Arabidopsis* seedlings were grown on agar media containing H_2O, 90 mM mannitol, or 90 mM sucrose and entrained under L12/D12 cycles for 10 d before transfer to DD for 60 h. Luminescence was quantified for 60 s in a luminometer to obtain basal activity. Cold treatment was then administered for 2 h (dark red bars), 3 h (orange bars), or 6 h (green bars), and the seedlings were then left for 15 min at 19 °C before quantifying luminescence for 240 s. Bars indicate average of cold-induced luminescence divided by basal luminescence for each condition. Error bars indicate the SEM (n = 12).

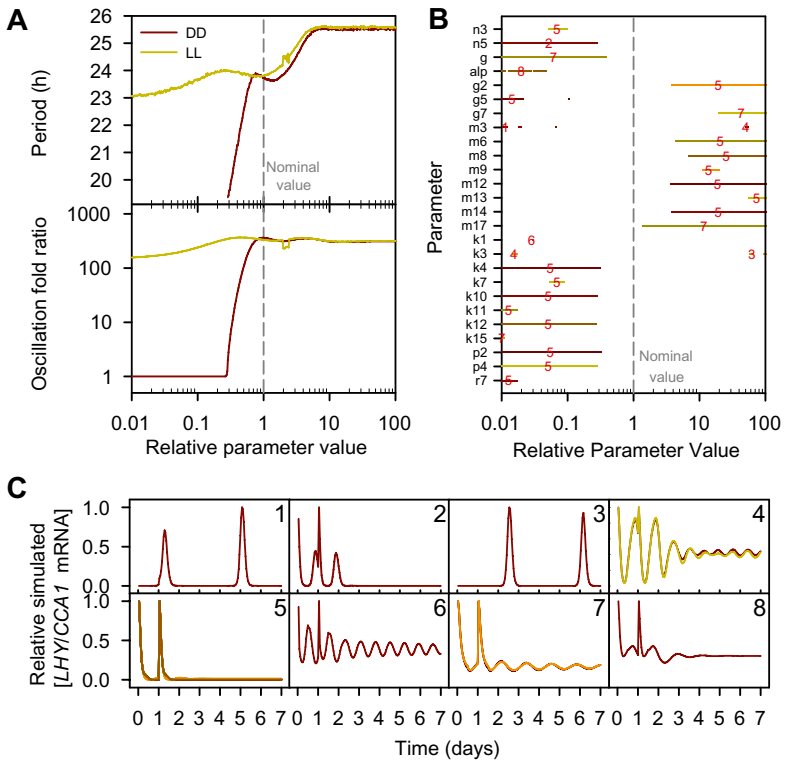

Fig. S2. Single-parameter alterations to the three-loop model can account for no exogenous sucrose. (*A*) Period and oscillation fold ratio of the three-loop model (1) in constant light (LL) and constant dark (DD) plotted as a function of the relative value of n_5 (maximum light-independent rate of *Y/GI* transcription), keeping all other parameters at their nominal value. (*B*) Relative parameter values for which LL period between 20 h and 30 h and DD oscillation fold ratio <1.1 are indicated. Overlaid red numbers located at the median value of each candidate range of increases or decreases refer to the clustered output in C. (*C*) Simulated [*LHY/CCA1* mRNA] for candidate values in *B* classified into eight clusters using the *kmeans* function in the Statistics Toolbox for MATLAB (4). Candidate values were taken to be the median values in the candidate range, as indicated in *B*. The line colors correspond to the parameter alterations in *B*. The model equations were solved numerically using MATLAB's *ode15s* stiff equation solver (2).

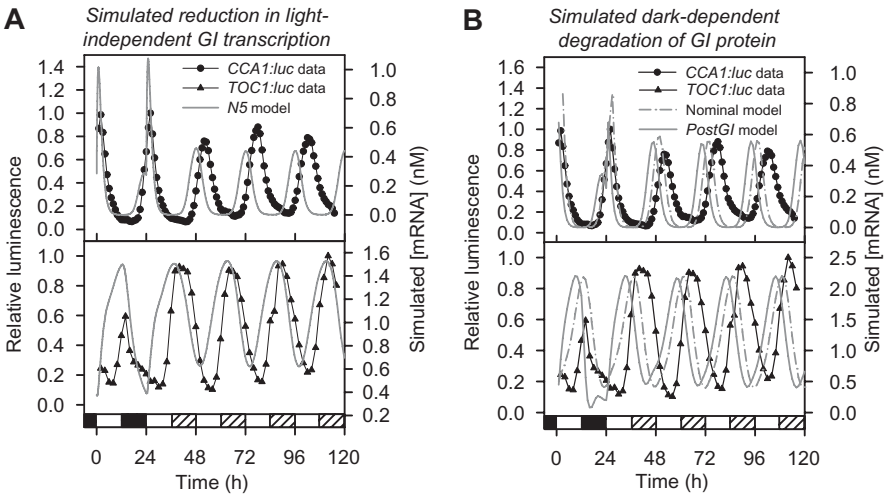

Fig. S3. Simulated gene expression in LL for the three-loop model altered for no exogenous sucrose. Relative *CCA1::luc* (solid circles, *Upper*) and *TOC1::luc* (solid triangles, *Lower*) luminescence in LD and LL were compared against equivalent simulated [*LHY/CCA1* mRNA] and [*TOC1* mRNA] (solid lines) from variants of the three-loop model. Data points are averages of clusters of 10–12 seedlings, quantified for 800 s with a photon counting camera. (*A*) *N5* is the three-loop model with the maximum rate of light-independent *Y* (*GI*) transcription (n_5) reduced to 0.25 of its nominal value. (*B*) *PostGI* is the three-loop model with increased maximum degradation of cytoplasmic and nuclear Y (GI) protein in the absence of light to five times the nominal rate. Bars on the abscissa are open for light, solid for darkness, and hatched for light in subjective night.

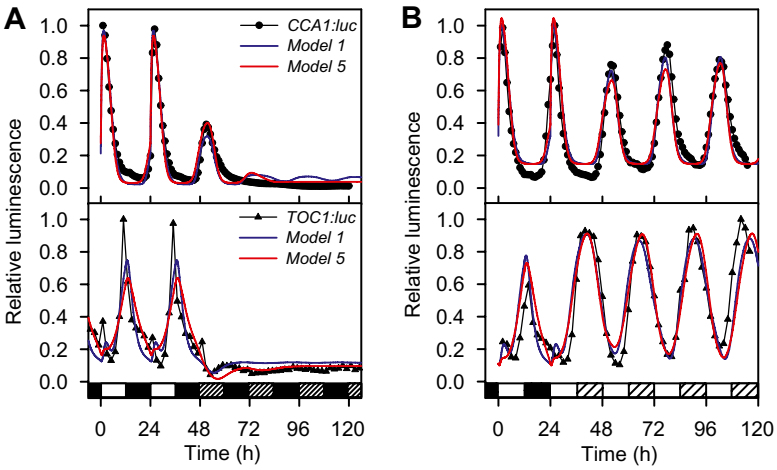

Fig. S4. Reoptimization of the three-loop model parameters enables accurate prediction of *CCA1* and *TOC1* expression in LL and DD. Comparison of annealed parameter sets from the Metropolis–Hastings algorithm is shown with *luc* luminescence data used in the cost function. Entrainment and measurement are shown in 12 h light, 12 h dark (LD12/12) cycles before transfer to (*A*) DD or (*B*) LL, for 96 h. *Model 1* (blue line) and *Model 5* (red line) simulations are compared against relative *CCA1::luc* (open circles) and *TOC1::luc* (open triangles) luminescence. Data points are averages of clusters of 10–12 seedlings, quantified for 800 s with a photon counting camera. *Model 1* corresponds to the parameter set with lowest cost function during optimization and displays low amplitude oscillations in DD. *Model 5* was the fifth lowest cost parameter set, although it was the lowest cost model that tends to steady state in DD. Parameter values for these models can be found in Table S2. Model equations were solved numerically using MATLAB's *ode15s* stiff equation solver (2). Bars on the abscissa are open for light, solid for darkness, and hatched for dark in subjective day (*A*) or light in subjective night (*B*).

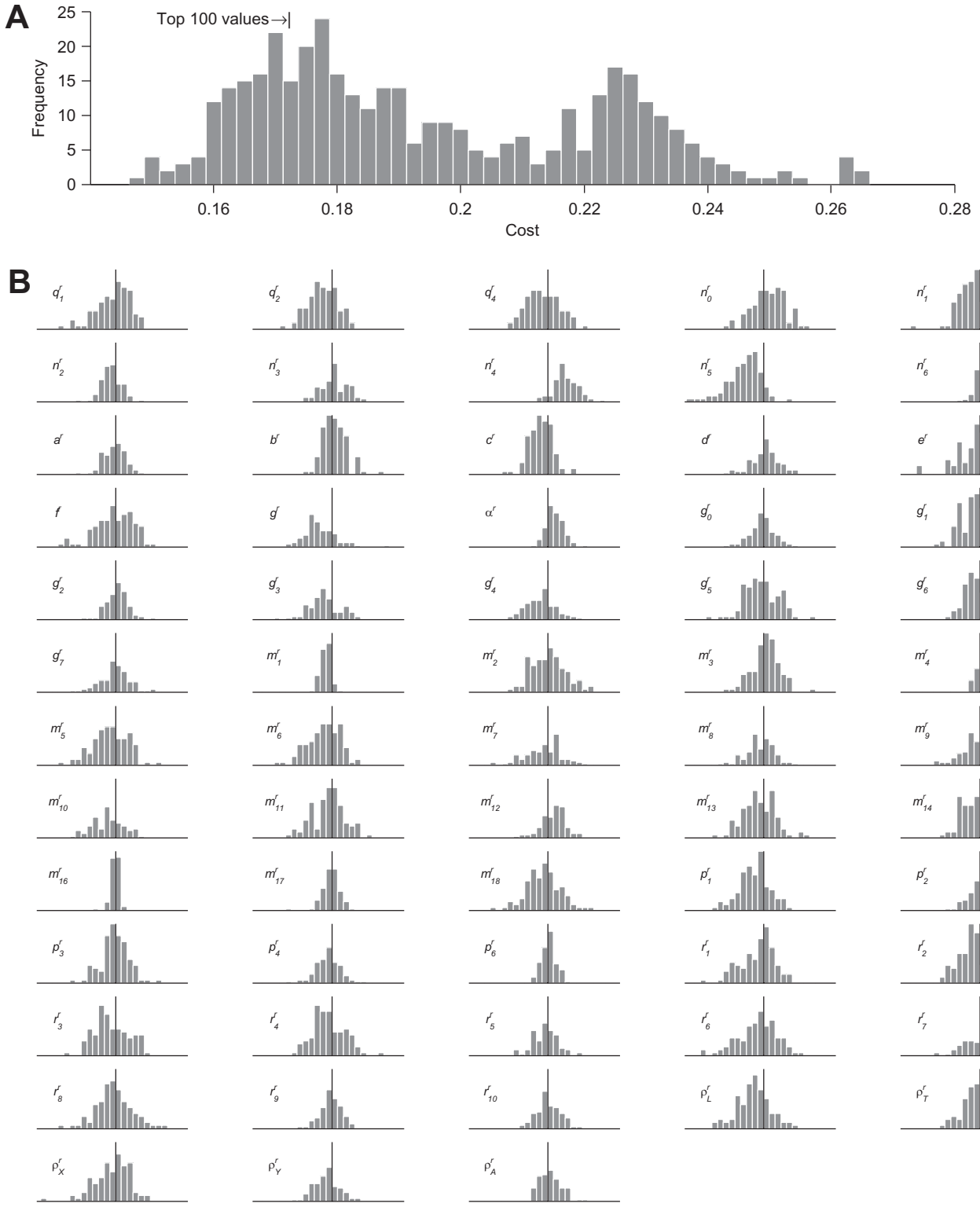

Fig. S5. Distributions of trial optimal solutions following reoptimization of the three-loop model. The parameters of the three-loop model were reoptimized against experimental data measuring *Arabidopsis* seedlings grown in the absence of exogenous sucrose. A Metropolis–Hastings simulated annealing algorithm was run 400 times, and the optimal cost parameter sets were retained for further analysis. (*A*) The histogram shows the bimodal distribution of cost function value among trial optimal parameter sets. A cutoff (indicated) was imposed for further analyzing the parameter values that must be modified to account for the absence of exogenous sucrose. (*B*) The histograms show the distribution of each relative parameter value (on a base-10 logarithmic scale), over the best 100 trial optimal parameter sets.

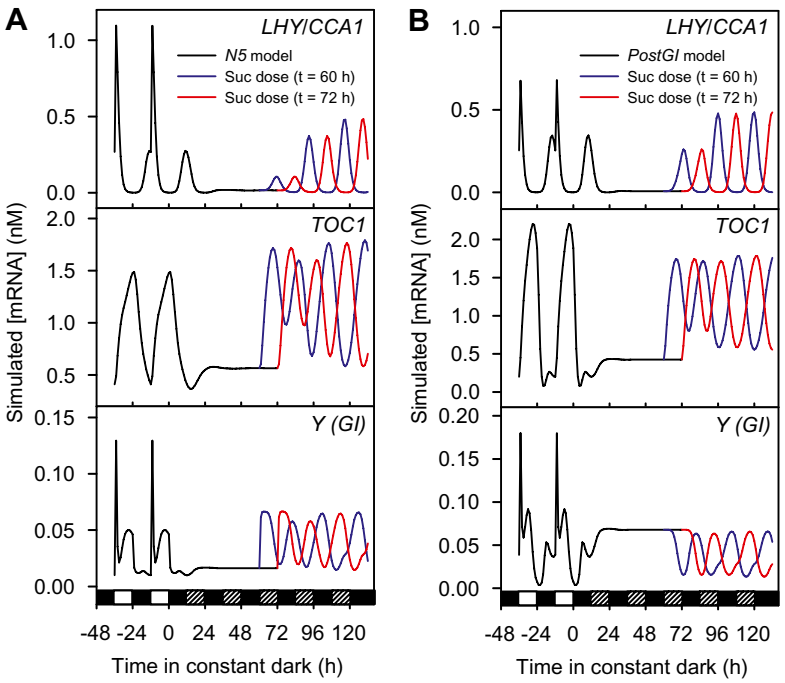

Fig. S6. Mathematical simulation of sucrose treatment in constant dark: Simulated [*LHY/CCA1* mRNA] (*Top*), [*TOC1* mRNA] (*Middle*), and [*Y* (*GI*) mRNA] (*Bottom*) in entrained LD12/12 cycles before transfer to DD. Simulations reflect alterations to the three-loop model (1) to account for no exogenous sucrose (black trace) before switching to the nominal (exogenous sucrose) model at $t = 60$ h (blue lines) or $t = 72$ h (red lines). Model equations were solved numerically using MATLAB's *ode15s* stiff equation solver (2). (*A*) *N5* model defined as the three-loop model with maximum light-independent rate of *Y* (*GI*) transcription (n_5) set to 0.25 of the nominal value. (*B*) *PostGI* model defined as the three-loop model but with the maximum degradation rates of cytoplasmic and nuclear Y (GI) protein $(\hat{m}_{13}, \hat{m}_{14})$ increased to five times the nominal value during darkness (i.e., $d = 5$ in Eq. **S24**). Bars on the abscissa are open for light, solid for darkness, and hatched for dark in subjective day.

Table S1. Parameter values and process descriptions for the three-loop model, adapted from ref. 1

Name	Value	Description
q_1	4.1954	Coupling constant of light activation of LHY transcription
n_0	0.05	Maximum light-dependent LHY transcription rate
g_0	1.0	Constant of repression by APRR7/9
α	4.0	Hill coefficient of repression by APRR7/9
n_1	7.8142	Maximum light-independent LHY transcription rate
a	1.2479	Hill coefficient of activation by protein X
g_1	3.1383	Constant of activation by protein X
m_1	1.999	Maximum rate of LHY mRNA degradation
k_1	2.392	Michaelis constant of LHY mRNA degradation
p_1	0.8295	Rate constant of LHY mRNA translation
r_1	16.8363	Rate constant of LHY transport into nucleus
r_2	0.1687	Rate constant of LHY transport out of nucleus
m_2	20.4400	Maximum rate of cytoplasmic LHY degradation
k_2	1.5644	Michaelis constant of cytoplasmic LHY degradation
m_3	3.6888	Maximum rate of nuclear LHY degradation
k_3	1.2765	Michaelis constant of nuclear LHY degradation
n_2	3.0087	Maximum TOC1 transcription rate
b	1.0258	Hill coefficient of activation by protein Y
g_2	0.0368	Constant of activation by protein Y
g_3	0.2658	Constant of repression by LHY
c	1.0258	Hill coefficient of repression by protein Y
m_4	3.8231	Maximum rate of TOC1 mRNA degradation
k_4	2.5734	Michaelis constant of TOC1 mRNA degradation
p_2	4.3240	Rate constant of TOC1 mRNA translation
r_3	0.3166	Rate constant of TOC1 transport into nucleus
r_4	2.1509	Rate constant of TOC1 transport out of nucleus
m_5	0.0013	Maximum rate of light-dependent cytoplasmic TOC1 degradation
m_6	3.1741	Maximum rate of light-independent cytoplasmic TOC1 degradation
k_5	2.7454	Michaelis constant of cytoplasmic TOC1 degradation
m_7	0.0492	Maximum rate of light-dependent nuclear TOC1 degradation
m_8	4.0424	Maximum rate of light-independent nuclear TOC1 degradation
k_6	0.4033	Michaelis constant of nuclear TOC1 degradation
n_3	0.2431	Maximum transcription rate of protein X
d	1.4422	Hill coefficient of activation by TOC1
g_4	0.5388	Constant of activation by TOC1
m_9	10.1132	Maximum rate of degradation of protein X mRNA
k_7	6.5585	Michaelis constant of protein X mRNA degradation
p_3	2.1470	Rate constant of X mRNA translation
r_5	1.0352	Rate constant of protein X transport into nucleus
r_6	3.3017	Rate constant of protein X transport out of nucleus
m_{10}	0.2179	Maximum rate of degradation of cytoplasmic protein X
k_8	0.6632	Michaelis constant of cytoplasmic protein X degradation
m_{11}	3.3442	Maximum rate of degradation of nuclear protein X
k_9	17.1111	Michaelis constant of nuclear protein X degradation
q_2	2.4017	Coupling constant of light activation of Y mRNA transcription
n_4	0.0857	Light-dependent component of Y transcription
n_5	0.1649	Light-independent component of Y transcription
g_5	1.1780	Constant of repression by TOC1
g_6	0.0645	Constant of repression by LHY
e	3.6064	Hill coefficient of repression by TOC1
f	1.0237	Hill coefficient of repression by LHY
m_{12}	4.2970	Maximum rate of degradation of protein Y mRNA
k_{10}	1.7303	Michaelis constant of protein Y mRNA degradation
p_4	0.2485	Rate constant of Y mRNA translation
r_7	2.2123	Rate constant of protein Y transport into nucleus
r_8	0.2002	Rate constant of protein Y transport out of nucleus
m_{13}	0.1347	Maximum rate of degradation of cytoplasmic protein Y
k_{11}	1.8258	Michaelis constant of cytoplasmic protein Y degradation
m_{14}	0.6114	Maximum rate of degradation of nuclear protein Y
k_{12}	1.8066	Michaelis constant of nuclear protein Y degradation
p_5	0.5000	Light-dependent production of protein P
k_{13}	1.2000	Michaelis constant of protein P degradation

Table S1. Cont.

Name	Value	Description
m_{15}	1.2000	Maximum rate of protein P degradation
q_3	1.0000	Coupling constant of light activation of protein P degradation
q_4	2.4514	Coupling constant of light activation of LHY transcription
g	1.0258	Hill coefficient of activation by LHY
n_6	8.0706	Maximum light-independent APRR7/9 transcription rate
g_7	0.0004	Constant of activation by LHY
m_{16}	12.2398	Maximum rate of APRR7/9 mRNA degradation
k_{14}	10.3617	Michaelis constant of APRR7/9 mRNA degradation
p_6	0.2907	Rate constant of APRR7/9 mRNA translation
r_9	0.2528	Rate constant of APRR7/9 protein movement out of nucleus
r_{10}	0.2212	Rate constant of APRR7/9 protein movement into the nucleus
m_{17}	4.4505	Maximum rate of degradation of cytoplasmic protein APRR7/9
k_{15}	0.0703	Michaelis constant of cytoplasmic protein APRR7/9 degradation
m_{18}	0.0156	Maximum rate of degradation of nuclear protein APRR7/9
k_{16}	0.6104	Michaelis constant of cytoplasmic protein APRR7/9 degradation

Table S2. Average parameter alterations from fine-tuning

Parameter	Mean value	Model 1	Model 5	Parameter	Mean value	Model 1	Model 5
q_1^r	1.0503	1.1620	1.8689	m_7^r	1.0258	1.4205	0.3447
q_2^r	0.8299	0.1930	0.6184	m_8^r	0.9800	1.0212	1.0498
q_4^r	0.9871	1.2855	1.5719	m_9^r	0.9412	1.3556	0.7569
n_0^r	1.3365	0.6599	0.9832	m_{10}^r	0.8828	0.7353	0.9643
n_1^r	0.8816	0.3931	0.6578	m_{11}^r	1.0052	1.1935	0.9847
n_2^r	0.9116	0.7852	0.8166	m_{12}^r	1.2952	1.6672	1.3404
n_3^r	1.1820	2.3971	2.6644	m_{13}^r	1.0021	1.0295	0.8325
n_4^r	1.9340	1.3212	2.0471	m_{14}^r	0.9562	1.0243	0.5075
n_5^r	0.6111	0.5990	0.3222	m_{16}^r	0.9832	1.2139	0.9445
n_6^r	1.0399	1.2228	0.9435	m_{17}^r	1.0119	0.6810	1.1407
a^r	1.0264	1.1040	0.6665	m_{18}^r	1.0150	1.5128	1.4185
b^r	1.1956	2.1621	1.6100	p_1^r	0.8336	0.6290	0.4971
c^r	0.8515	1.3502	1.6279	p_2^r	1.1152	1.4066	1.1454
d^r	1.1559	0.7824	1.6591	p_3^r	1.0755	1.2930	0.5408
e^r	1.0435	1.2389	1.4814	p_4^r	0.9562	0.8127	1.0030
f^r	1.1175	1.6439	1.0295	p_6^r	1.0728	0.8485	1.1129
g^r	0.7947	0.5568	0.7329	r_1^r	0.9395	0.8686	0.6608
α^r	1.3087	1.5077	1.4316	r_2^r	0.9396	0.3801	0.5359
g_0^r	1.0318	1.4030	1.4133	r_3^r	1.0158	0.5565	1.1744
g_1^r	0.9721	1.1038	1.0409	r_4^r	1.0477	0.6094	1.1017
g_2^r	1.1200	0.8166	1.1862	r_5^r	1.0054	1.4205	0.7415
g_3^r	0.8869	1.2856	0.7802	r_6^r	0.9748	0.6103	1.7480
g_4^r	0.8960	0.7379	0.3949	r_7^r	1.1355	0.6581	2.2134
g_5^r	1.0814	0.8031	0.6612	r_8^r	1.1156	0.5266	1.1484
g_6^r	1.1526	1.8767	0.7370	r_9^r	1.0142	1.1112	1.0065
g_7^r	1.1029	1.1953	0.4917	r_{10}^r	1.0975	1.1925	0.7078
m_1^r	0.8255	0.7560	1.0997	ρ_L^r	0.8288	0.7413	0.7910
m_2^r	1.1963	0.7207	0.9365	ρ_T^r	1.0837	1.3384	1.0044
m_3^r	1.1778	1.2693	1.5396	ρ_X^r	1.0252	0.9911	0.7587
m_4^r	1.2465	1.3819	1.3328	ρ_Y^r	0.9180	0.9219	0.8465
m_5^r	0.9870	1.5939	0.9055	ρ_A^r	1.1415	0.9196	1.1095
m_6^r	0.8862	0.1991	0.8877				

A Metropolis–Hastings algorithm was used to refine the nondimensionalized three-loop model parameters, on the basis of *CCA1::luc* and *TOC1::luc* luminescence data. The algorithm was run 1,000 times, and the lowest-cost parameter set was retained as an annealed parameter set. The relative values of the top 100 annealed parameter sets were averaged to assess which parameters should be changed to account for no exogenous sucrose. The logarithm of these values is plotted in Fig. 3*B* in the main text. Model 1 corresponds to the annealed parameter set with lowest cost function value. Model 5 has the fifth lowest cost overall, but is the lowest-cost model that tends to steady state in DD. The tabulated values correspond to the relative parameter values defined in Table S2.

Table S3. Rescaled parameters for the nondimensionalized version of the three-loop model

Name	Definition	Value	Name	Definition	Value
$\hat{q}_1$	q_1/k_1	1.7539	$\hat{p}_3$	p_3k_7/k_8	21.2321
$\hat{n}_0$	n_0/k_1	0.0209	$\hat{r}_6$	r_6k_9/k_8	85.1865
$\hat{g}_0$	g_0/k_{16}	1.6383	$\hat{m}_{10}$	m_{10}/k_8	0.3286
$\hat{n}_1$	n_1/k_1	3.2668	ρ_X	k_8/k_9	0.0388
$\hat{g}_1$	g_1/k_9	0.1834	$\hat{m}_{11}$	m_{11}/k_9	0.1954
$\hat{m}_1$	m_1/k_1	0.8357	$\hat{q}_2$	q_2/k_{10}	1.388
$\hat{p}_1$	p_1k_1/k_2	1.2683	$\hat{n}_4$	n_4/k_{10}	0.0495
$\hat{r}_2$	r_2k_3/k_2	0.1377	$\hat{n}_5$	n_5/k_{10}	0.0953
$\hat{m}_2$	m_2/k_2	13.0657	$\hat{g}_5$	g_5/k_6	2.9209
ρ_L	k_2/k_3	1.2255	$\hat{g}_6$	g_6/k_3	0.0505
$\hat{m}_3$	m_3/k_3	2.8898	$\hat{m}_{12}$	m_{12}/k_{10}	2.4834
$\hat{n}_2$	n_2/k_4	1.1692	$\hat{p}_4$	p_4k_{10}/k_{11}	0.2355
$\hat{g}_2$	g_2/k_{12}	0.0204	$\hat{r}_8$	r_8k_{12}/k_{11}	0.1981
$\hat{g}_3$	g_3/k_3	0.2082	$\hat{m}_{13}$	m_{13}/k_{11}	0.0738
$\hat{m}_4$	m_4/k_4	1.4856	ρ_Y	k_{11}/k_{12}	1.0106
$\hat{p}_2$	p_2k_4/k_5	4.0531	$\hat{m}_{14}$	m_{14}/k_{12}	0.3384
$\hat{r}_4$	r_4k_6/k_5	0.316	$\hat{q}_4$	q_4/k_{14}	0.2366
$\hat{m}_5$	m_5/k_5	0.0005	$\hat{n}_6$	n_6/k_{14}	0.7789
ρ_T	k_5/k_6	6.8073	$\hat{g}_7$	g_7/k_3	0.0003
$\hat{m}_6$	m_6/k_5	1.1562	$\hat{m}_{16}$	m_{16}/k_{14}	1.1813
$\hat{m}_7$	m_7/k_6	0.122	$\hat{p}_6$	p_6k_{14}/k_{15}	42.847
$\hat{m}_8$	m_8/k_6	10.0233	$\hat{r}_{10}$	$r_{10}k_{16}/k_{15}$	1.9206
$\hat{n}_3$	n_3/k_7	0.2431	$\hat{m}_{17}$	m_{17}/k_{15}	63.3073
$\hat{g}_4$	g_4/k_6	1.336	ρ_A	k_{15}/k_{16}	0.1152
$\hat{m}_9$	m_9/k_7	1.542	$\hat{m}_{18}$	m_{18}/k_{16}	0.0256

The number of parameters in the three-loop model was reduced by dividing each state variable (x_i) by its corresponding Michaelis constant of degradation (k_i) for all i (Eqs. S2–S17). The resulting parameter set corresponding to the nominal configuration is tabulated.